*Revised manuscript (unmarked)
Click here to view linked References

Nitrogen-induced reconstructions on the Cr(001) surface

Emiliano Ventura-Macias[a,b], J. Guerrero-Sánchez[a], J. P. Corbett[c,1], A. R. Smith[c], and Noboru Takeuchi[a]

[a] *Centro de Nanociencias y Nanotecnología, Universidad Nacional Autónoma de México, Apartado Postal 14, Ensenada, Baja California, Código Postal 22800, México.*

[b] *Posgrado en Nanociencias, Centro de Investigación Científica y Estudios Superiores de Ensenada, Carretera Ensenada-Tijuana No. 3918, Zona Playitas, CP. 22860, Ensenada, B.C., México.*

[c] *Department of Physics and Astronomy, Nanoscale and Quantum Phenomena Institute, Ohio University, Athens, Ohio 45701*

Abstract

We use spin-polarized density functional theory to describe the surface reconstructions formed when the Cr(001) surface is exposed to nitrogen. Our primary goal is to clarify the atomic structure of the N induced c(2x2) Cr(001) reconstruction and to study its properties. After analyzing the relative stability of several models with a ½ monolayer of N atoms on the surface, it was found that only two models were stable for different growth conditions. The first stable model shows two N atoms (per cell) adsorbed on hollow sites following a diagonal pattern. In the second, N atoms replace Cr atoms of the first monolayer, and after optimization, they end up in almost second layer positions. To compare with scanning tunneling microscopy experiments, simulated STM images, using the Tersoff-Hamann approximation, were obtained. Our two models can explain the two different c(2x2) Cr(001) reconstructions observed experimentally. The magnetic properties, such as magnetic moments and alignments, are discussed compared with experimental values.

[1] Current address: Department of Physics, The Ohio State University, Columbus, OH 43210, USA

Keywords: Surface reconstructions, STM images, Antiferromagnetic alignment.

1. Introduction

Chromium (001) surfaces have been widely studied because of their applications in catalysis, and as an anti-corrosion material [1, 2]. They also have important electronic properties, such as a sharp resonance close to the Fermi level, which has been observed in angular resolved photo-emission experiments [3], and studied by first-principles calculations [4]. Furthermore, Cr(001) has promising magnetic properties, like a topological antiferromagnetic order between the surface layers [5]. This magnetic arrangement can result in remarkable physical effects when the Cr(001) surface is interfaced with other magnetic materials, such as Fe [6]. These Cr(001)-based heterostructures could display an exchange bias effect, and therefore, they could be used in the next generation of magnetic storage devices. However, pristine Cr(001) surfaces are very difficult to obtain as it readily adsorbs contaminants [7]. Initially, the motivation to study the adsorption of C, N, and O on Cr(001) surface was to understand the effects of impurities on the surface structure. Upon adsorption, ad-atoms and surface atoms rearrange themselves to achieve their minimum energy structure, forming surface reconstructions. These new configurations also modify the properties of the surface. Such changes are very important when devices are fabricated at the nanoscale. Therefore, a correct atomic description of these surface reconstructions is mandatory.

The modification of the Cr(001) surface with adatoms like Fe, C, O, and N, has been studied previously [6-8]. In the case of N, several reconstructions have been found upon nitrogen dosing, being the p(1×1), the c(2×2), and the c(3√2×√2)R±45 [1-9] the most common ones.

The interest to study the N adsorption on Cr(001) has recently increased, because of the potential formation of CrN on Cr(001) layers. Chromium nitride thin films have been widely studied because of their mechanical properties, such as high hardness. Also, CrN is considered as a material for electronic devices due to its semiconductor behavior [10]. Moreover, recently, it has been studied as a spintronic material because of its magnetic phase transitions [11-13], and as an energy-harvesting material because of its thermoelectric properties [14].

It has been shown that a transition layer is formed at the CrN/Cr interface, which has been identified as hexagonal Cr_2N [15]. We have to point out that in the surface reconstructions induced by N, there is probably a single layer of CrN while in Ref. [15] there are several layers. However, it is interesting to notice that the Cr/N ratio at the interface in the samples of Ref [15] is the same as in the surface reconstructions.

In this paper we are interested in studying the c(2×2) reconstruction induced by N adsorption. This surface was previously studied using Auger spectroscopy and scanning tunneling microscopy. Based on the experiments, an atomic model was proposed. Recently, J. P. Corbett and A. R. Smith [9] reported that Nitrogen gas left in the Molecular Beam Epitaxy chamber induces a c(2x2) reconstruction, but they could not relate it to the reconstruction reported in [8]. As their results confirm a layer-wise antiferromagnetic spin structure with the quantification of a 180º spin reversal between Cr(001) layers, it is of interest to describe the atomic structure of the reconstruction they found.

Considering the previous discussion, using first-principles calculations, we have investigated the c(2x2) reconstruction formed by the adsorption of N atoms on the Cr(001) surfaces. Different from early reports, we have found two c(2x2) surface structures. We have also calculated STM

images of the two configurations using the Tersoff Hamman approximation. It is found that images using the model proposed in Ref. [8] cannot explain their own STM images but can explain the new STM experiments of Ref. [9]. On the other hand, calculated STM images of our second model explain well the images of Ref. [8].

The rest of our paper is organized as follows: in section 2 we describe the computational method, in section 3 we discuss the main results and compare with some experimental STM images, and finally, in section 4 we make some conclusions.

2. Method

2.1 Calculation parameters

First-principles, spin-polarized calculations were carried out within the density-functional theory. The Quantum ESPRESSO's plane-wave self-consistent code was used for the calculations [16]. The exchange-correlation energy was treated with the generalized gradient approximation as stated by Perdew–Burke–Ernzerhof [17]. The nucleus and core electrons were replaced with Vanderbilt's ultrasoft pseudopotentials [18]. The Kohn-Sham electronic states were expanded with a kinetic energy cutoff of 30 Ry. The charge density cutoff energy follows the relation of 8-times the kinetic energy cutoff. The Brillouin zone was sampled with an equally spaced 4×4×1 k-points grid mesh.

The scanning tunneling microscopy (STM) images were calculated with the Tersoff & Hamann approximation [19] as implemented on Quantum ESPRESSO. The bias voltage was set following the experiment at -0.325 V (to describe occupied states). The tip-to-surface distances were defined between 2 and 3 Å, similar to those used in the experiment.

2.2 Experimental setup

The experiments were performed in ultra-high vacuum (UHV) conditions with base pressures of 1.0×10^{-10} Torr with samples prepared via molecular beam epitaxy (MBE). The STM and MBE are coupled in UHV allowing for *in-situ* growth and scanning under UHV conditions. The STM is operated in constant current mode with a 0.1 nA setpoint current.

2.3 Model setup

We have first optimized the body-centered cubic structure of chromium, in a Type-A antiferromagnetic (aFM) alignment, along [001]. Density-functional theory does not take temperature into account, so calculations are performed at 0 K. The calculated value of 2.90 Å for the lattice constant slightly overestimate with the experimental parameter (2.88 Å) [20], which is to be expected for the GGA approximation [21].

To construct the Cr(001) surface, we have taken advantage of the inversion symmetry of the Cr lattice, and two equivalent surfaces of (2×2) Cr(001) have been generated with 7 layers each. To avoid surface-to-surface interactions we left a vacuum of ~20□. The constructed supercell conserves its bulk out-of-plane aFM behavior. The calculated surface magnetic moment is 2.7μ_B, which is in good agreement with the 2.6 $\mu_B$value of other GGA calculations [22].

To study the adsorption and incorporation of N atoms on the Cr surface, we have considered four high symmetry adsorption sites: top, bridge, hollow, and Cr/N exchange (N atoms taking first layer Cr positions) sites. We focused on models containing ¼ and ½ monolayers of N atoms, as experimental evidence [8, 14] shows that they are the most common. The (2×2) supercell that we have used is the smallest where three main reconstructions can be formed with these coverages: p(2×2), p(2×1), and c(2×2). However, the p(2x1) was not considered because in the experimental images there was no evidence of a reconstruction showing parallel-lines.

Also, as stated by Sporn et al. [8], full N monolayer in hollow sites may be stable. Therefore, we also included the p(1×1)-h-N reconstruction in the calculations. Finally, we also considered a ½

monolayer Chromium surface with Cr vacancies in the c(2x2)-v-Cr model, since it may appear for poor Cr conditions.

3. Results and Discussion

In this section, we describe the atomic arrangement of the proposed models and their thermodynamic stability. We also compare the theoretical Tersoff-Hamann STM (TH-STM) simulations of the most stable structures with the experimental images. Lastly, we discuss the spin densities and magnetic moments of the most relevant structures.

3.1 Structural details

We first consider the adsorption of ¼ ML atoms at high symmetry sites shown in Fig. 1a, to understand the structural characteristics of each of these sites. After structural relaxation by energy minimization, the nitrogen at the top site (t) lingers above a first-layer chromium at 1.58 Å. In the two-fold bridge position (b), N is between adjacent first layer chromium atoms, and at 1.34 Å above. The hollow site (h) has a fourfold symmetry, laying precisely in the middle of four chromium atoms of the first monolayer, the nitrogen atom is at 0.41 Å above the surface. This result agrees with the literature [8], as seen in Fig. 2a. By optimizing the atomic coordinates and computing the total energy of each model with the same number of atoms, we ruled out the Top and Bridge sites, since their energies were considerably higher than the H4-site by 2.57 and 1.42 eV/(N-adatom), respectively.

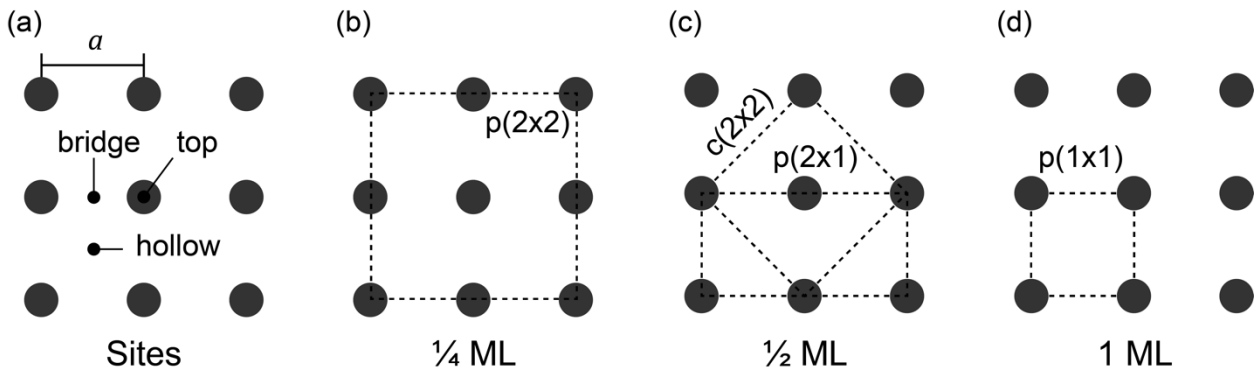

Figure 1. Chromium (001) surface (a) high symmetry sites. Possible reconstructions in a 2x2 supercell for (b) ¼ monolayer N coverage, (c) ½ monolayer N coverage, and (d) a full N monolayer.

In the case of ¼ ML, we can only observe the p(2x2) reconstruction in our supercell, as shown in Fig. 1b. For the ½ ML, we can either observe a c(2x2) or a p(2x1) reconstruction. We dismissed the p(2x1) reconstruction by comparing the relative energies of the two reconstructions for each site. As seen in Table 1, the c(2x2) reconstruction is the most favorable for every site. Also, current and past experimental results [2, 7, 8], are quick to dismiss the possibility of a p(2x1) reconstruction since its characteristic parallel lines do not show up in STM images. Lastly, for a full N ML coverage, we shall only consider the p(1x1) reconstruction.

Table 1. Relative energies for the two surface reconstructions induced by a ½ monolayer of N. The c(2x2) with N in hollow sites reconstruction is used as reference energy. Energies are in eV/(N adatom).

Reconstruction/Site	Top (t)	Bridge (b)	H4 (h)
p(2x1)	3.08	1.79	0.25
c(2x2)	2.89	1.73	0

These results also lead us to determine that the hollow site, for adsorbed N, is the most stable of the high symmetry sites. The c(2x2)-h-N model is the same as the one proposed by Sporn et al. [7]. We also note that in the Cr *bcc* structure these sites are directly above second-layer Cr atoms.

In typical growth conditions, incorporation of atoms into the substrate may occur. Therefore, we consider the possibility of N incorporation into inner layers. For this possibility, we propose that an N atom takes the place of a first-layer Cr atom (we will refer to this exchange as a substitutional (s) nitrogen). From the results, we found that the N sits at 1.32 Å beneath the first layer and 0.20 Å above the second layer, which is -almost- a second-layer H4-site adsorption. In Fig. 2 we compare the structural details of a hollow site N adsorption and a substitutional N adsorption. By comparing the distances in Fig. 2a and 2b, we can observe that the substitutional N does resemble a hollow site N in the second Cr layer, where the distance between N and the second later is $d_{N2} = 0.20$Å.

Evidence of N atoms being incorporated to second layer H4 sites has been previously speculated for the Cr(110) surface [2]. In Ref [2], the authors argued that reconstruction took place to let the N atom pass through first layer Cr atoms. However, they did not consider the possibility of N atoms taking the place of Cr atoms.

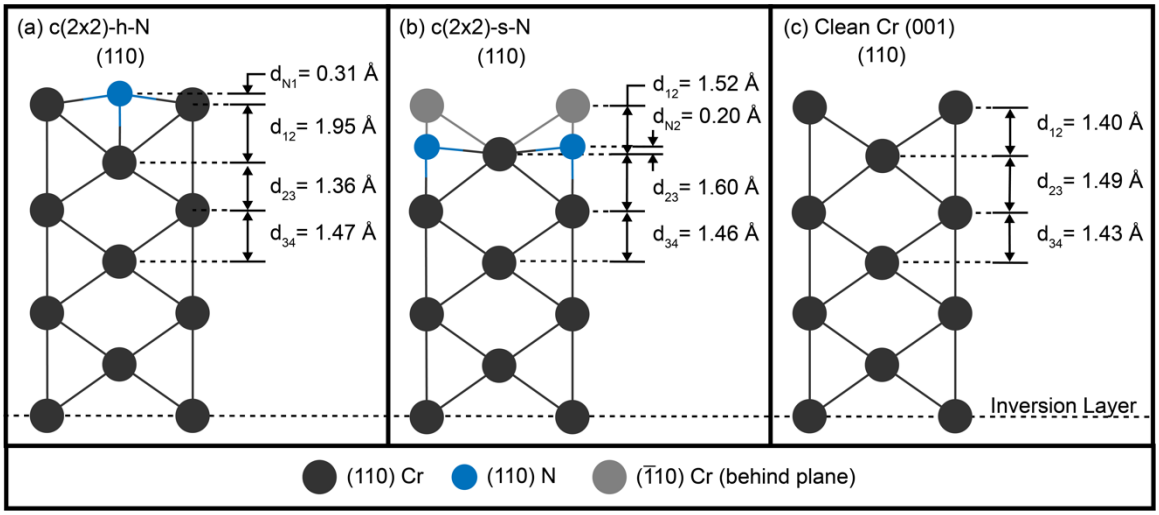

Figure 2. Side view along the (110) plane of the structures: (a) hollow and (b) substitutional sites, both corresponding to a c(2x2) reconstruction, and (c) to the clean Cr(001) surface.

To determine the most stable configurations of the sites and reconstructions, we have computed the surface formation energies (Ω) for each model, since most of them have a different number of atoms. We have computed Ω under rich and poor conditions of both N and Cr.

Following the results of the Ω's, we also calculated a model (c(2x2)-v-Cr) with vacant Cr sites to account for N-poor conditions in the substitutional N case.

3.2 Stability Analysis

To compare the stability of various models with a different number of atoms (0, ¼, ½, and 1 ML), we have used the surface formation energy (Ω) formalism [23-26]. By varying the chemical potentials of N and Cr (μ_N and μ_{Cr}, respectively), we have considered diverse growth conditions. For N dependence we vary μ_N and set Cr-rich conditions, and for Cr dependence, we vary μ_{Cr} and set N-rich conditions (see below for N and Cr rich conditions description).

Figure 3a shows the Ω, as a function of the N chemical potential (μ_N). When $\mu_N = 0.5 \times E_{N_2}$, we have nitrogen-rich conditions, we will call this upper limit μ_{N-mol} as it is the chemical potential of N in its molecular form. Decreasing μ_N is equivalent to a decrease of N content. The lower limit corresponds to the energy of the isolated N atom, with $\mu_N - \mu_{N-mol} > E_{N_{atom}} = -8.21\ eV$ (not shown in the figure). We can see that the Top and Bridge sites are less stable than the H4 and Substitutional geometries. For N-rich conditions, the most stable model corresponds to the full monolayer of N atoms occupying H4-sites (p(1x1)-h-N). When decreasing the nitrogen content, for $\Delta\mu_N = \mu_N - \mu_{N-mol} < -1.52\ eV$, the half-coverage of N at hollow sites becomes more favorable. This structure corresponds to a c(2x2)-h-N reconstruction model. For N-poor conditions ($\Delta\mu_N = \mu_N - \mu_{N-mol} < -2.31\ eV$) the most stable model is the clean Cr(001) surface, indicating that there are no N atoms at the surface anymore.

As mentioned before, nitrogen growth conditions consider only different nitrogen content, but not the case in which the chromium content is modified by an N/Cr exchange at the surface. To describe this situation, we must include chromium dependence, as shown in Fig. 3b, where we plot the Ω as a function of μ_{Cr}.When $\mu_{Cr} = \mu_{Cr-bulk}$, where $\mu_{Cr-bulk}$ is the energy per atom of the Cr bulk, we have chromium rich conditions. Decreasing μ_{Cr} is equivalent to a decrease of Cr content. The lower limit corresponds to the energy of the isolated Cr atom, with $\mu_{Cr} - \mu_{Cr-bulk} > E_{Cr_{atom}} = -4.10\ eV$ (not shown in the figure). From Cr-rich conditions to $\Delta\mu_{Cr} = \mu_{Cr} - \mu_{Cr-bulk} < -3.03\ eV$ the stable structure is the p(1x1)-h-N geometry with 1ML of N atoms at H4-sites. The c(2x2)-s structure is stable for poor Cr growth conditions. These results show that substitutional N models are stable and may exist experimentally.

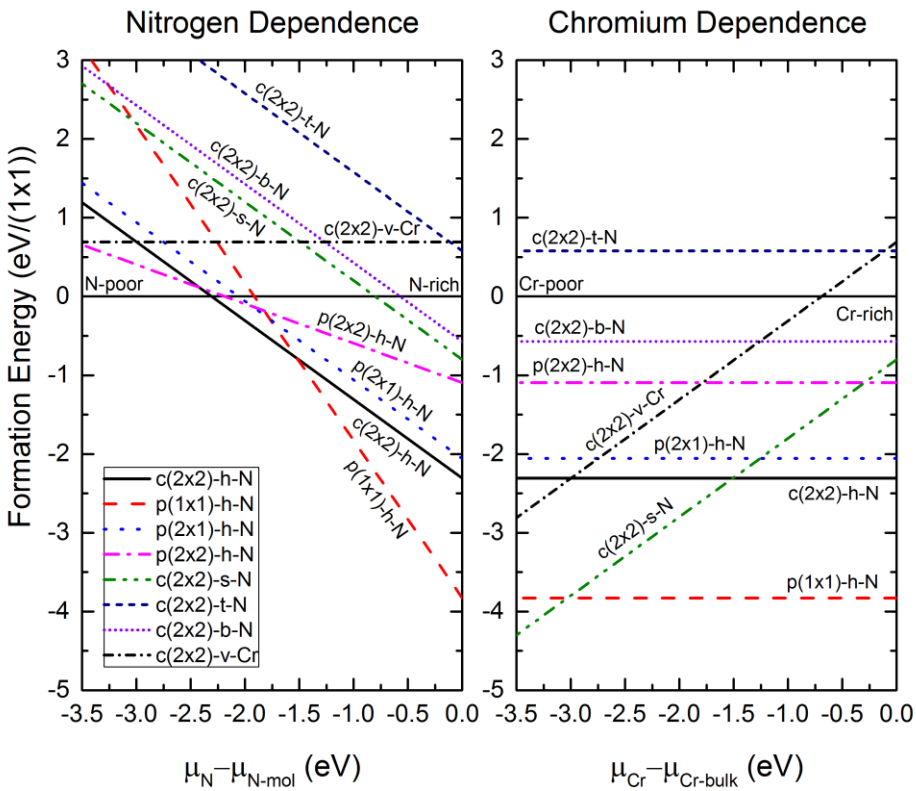

Figure 3. Surface formation energies for different conditions, varying (a) N and (b) Cr chemical potentials. For N dependence μ_{Cr} is set to the bulk value (Cr-rich conditions), and for Cr dependence, μ_N is set to half E_{N_2} (N-rich conditions).

To get the complete picture of the growth conditions for the most stable reconstructions, we have calculated a chemical-potential-based phase diagram. The Ω is shown as a color-map in the diagram.

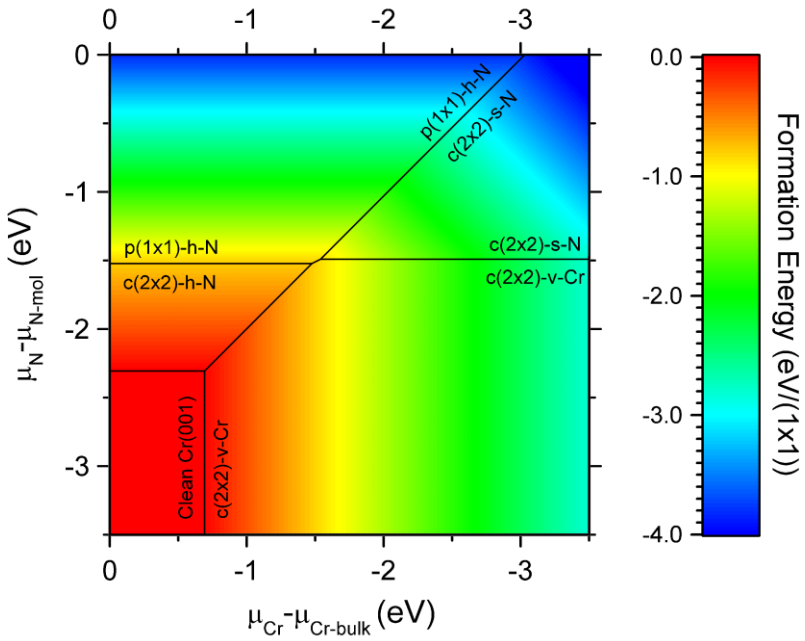

Figure 4. Phase diagram of the most stable reconstructions with a superimposed colormap of the Ω for each point in the diagram.

Firstly, we describe the dependence on N conditions. We can observe that for N-rich and Cr-rich conditions, the full monolayer reconstruction model, p(1x1)-h-N, is the most stable. As we go to N-poor conditions ($\Delta\mu_N < -1.52\ eV$), the ½ ML coverage reconstruction model, c(2x2)-h-N, becomes the most stable; this is due to the scarcity of N atoms, and also the reconstruction does not depend on Cr conditions. Towards the poorest N conditions ($\Delta\mu_N < -2.31 eV$), reconstructions with no N atoms are favored, and thus the clean Cr (001) surface is the most stable.

For the case of Cr dependence, the p(1x1)-h-N structure is by far the most stable. As we go to Cr-poor conditions, $\Delta\mu_{Cr} < -3.03\ eV$, the c(2x2)-s-N reconstruction model appears. For this

model, a particular behavior occurs: for certain combinations of Cr and N conditions it is the most stable. These combinations occur at Cr conditions up to $\Delta\mu_{Cr} = -1.54\ eV$, as long as the N conditions are sufficiently poor ($\Delta\mu_N > -1.49\ eV$, refer to Fig. 4 for graphic representation). These conditions mean that there always has to be Cr deficiency, as well as N deficiency, to have the N-for-Cr substitution and thus the c(2x2)-s-N reconstruction. As we go to very Cr-poor conditions, the c(2x2)-s-N model is stable, independent of the deficiency of N.

Finally, when Cr and N conditions are sufficiently poor, the c(2x2)-v-Cr reconstruction model becomes the most stable. When Cr is scarce, the top layer cannot be completed, and we have Cr vacancies. Furthermore, at the right N conditions, N will occupy the positions of the Cr vacancies in the second-layer at hollow sites, forming the c(2x2)-s-N reconstruction model.

3.3 Theoretical and experimental STM images

In order to describe which of the stable half-monolayer, c(2x2) reconstruction, models explain the previously reported and the new experimental findings; we proceed to simulate STM images using the Tersorff Hamman approximation (TH-STM). This simulation was done for the most stable models: c(2x2)-h-N, c(2x2)-s-N, and p(1x1)-h-N. Neither the ideally terminated surface nor the c(2x2)-v-Cr model was included, as the interest was to image the effect of N on the surface and they do not contain nitrogen atoms.

As discussed in Section 3.1, the c(2x2)-h-N reconstruction model (Fig. 2a) corresponds to a half coverage of N atoms located at H4-sites. In the c(2x2)-s-N reconstruction model (Fig. 2b), in the

topmost layer, half of the Cr atoms are substituted by N atoms. Lastly, the p(1x1)-h-N reconstruction model (Fig. 5c) has full coverage of N atoms in the H4-sites.

Interestingly, for the c(2x2)-h-N reconstruction model, simulated STM images (Fig. 5a) show that the bright spots are due to Cr atoms of the surface, whereas N atoms do not have a significant local density of states (LDOS), being the dark spots in the STM image. The LDOS of Cr appears to spread out to the unoccupied hollow sites, while in the N-occupied sides it appears as if N is preventing the Cr LDOS from spreading out.

The STM image for the c(2x2)-s-N reconstruction model (Fig. 5b) shows a pattern of bright spots (high local density of states) along the [110] direction, each four bright spots are separated by one dark spot which corresponds to a N atom on the same layer (in this structure half of the Cr atoms are substituted by N atoms).

Lastly, the p(1x1)-h-N reconstruction model (Fig. 5c), which has full coverage of N atoms in the H4-sites, forms a clear 1x1 pattern formed by four bright spots with one dark spot in the middle. It resembles the c(2x2)-s-N image but at half the scale and with the bright spots aligned with the [100] and [010] directions.

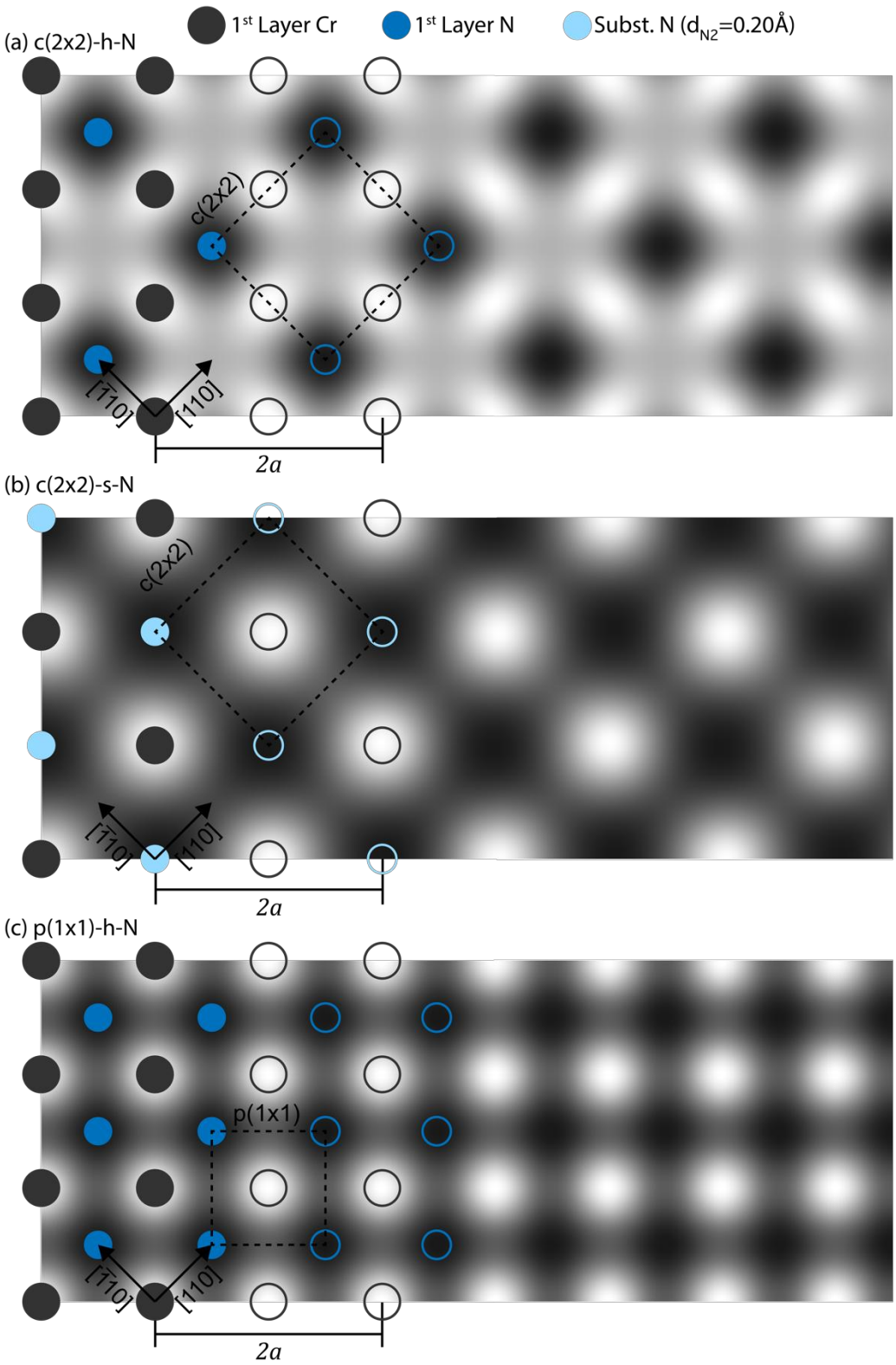

Figure 5. On the left-hand side, the reconstruction models are shown, while on the background and the right-hand side theoretical TH-STM images for the relevant reconstructions are shown.

The bias voltage is used as in the experiments, and the tip-to-surface distances were simulated at 2.5 Å.

From these results, we can relate the p(1x1)-h-N model with the (1x1) reconstruction reported by Sporn et al. [8]. To identify the c(2x2)-h-N and c(2x2)-s-N reconstructions, we show in Fig. 6 experimental STM images of the N-doped Cr(001) surface with two different c(2x2) reconstructions. The distance between dark spots in both images is approximately 4.2Å, this distance is very close to $\sqrt{2}a$ (4.1Å), which corresponds to the length of the sides of the c(2x2) reconstruction cell. We have superimposed a c(2x2) cell in the experimental images to show the lattice correspondence to the TH-STM images in the insets.

We can assign the experimental image in Fig. 6a to our c(2x2)-h-N (Fig. 5a). In this figure, large bright regions are imaged, showing the local density of states of the first-layer Cr atoms, whereas the dark spots (low local density of states) are generated by N atoms. These dark spots are precisely on the corners of the example reconstruction cells, whereas on the sides of the cells there is a major density of states from the Cr atoms. To confirm the subtle atomic positions in the c(2x2)-h-N structure, line profiles (Fig 6c) traversing the Cr-N-Cr positions (bright to dark to bright contrast) and the Cr-hollow-site-Cr positions (bright to medium to bright contrast) are taken along the red and black lines respectively in Fig. 6a. As expected from the TH-STM images for the 2 parallel experimental line profiles, the 2 profiles are out of phase with each other (peaks align with valleys and vice versa). Furthermore, Fig. 6(d-e) are 2-dimensional Fourier transforms (FT) of the experimental and Tersoff-Hamann STM images of the c(2x2)-h-N

structure. A square array with three k-points per side is anticipated and confirmed in the experimental FT.

Turning to the second c(2x2) experimental structure, a good match is seen between Fig. 6b and our c(2x2)-s-N TH-STM image (Fig. 5b), where the bright regions are now more localized on top of first layer Cr atoms and the second monolayer Cr atoms are not visible. The low local density of states regions (dark spots) are related to the substitutional N atoms near the second monolayer ($d_{N2} = 0.20$Å). Furthermore, the 2D FT of the c(2x2)-s-N is a simple square array of k-points as shown in Fig. 6(g-h) for experimental STM and TH-STM images, respectively. Line profiles across the STM image shown in Fig. 6(b) along the [110] direction for both Cr-Cr positions (red line) and N-N positions (black line) are displayed in Fig. 6(f) where it is seen that the 2 profiles are closely in phase (peaks align with peaks, valleys with valleys), as expected based on the TH-STM image of the c(2x2)-s-N structure, where the medium contrast arises from the bridge site between Cr atoms.

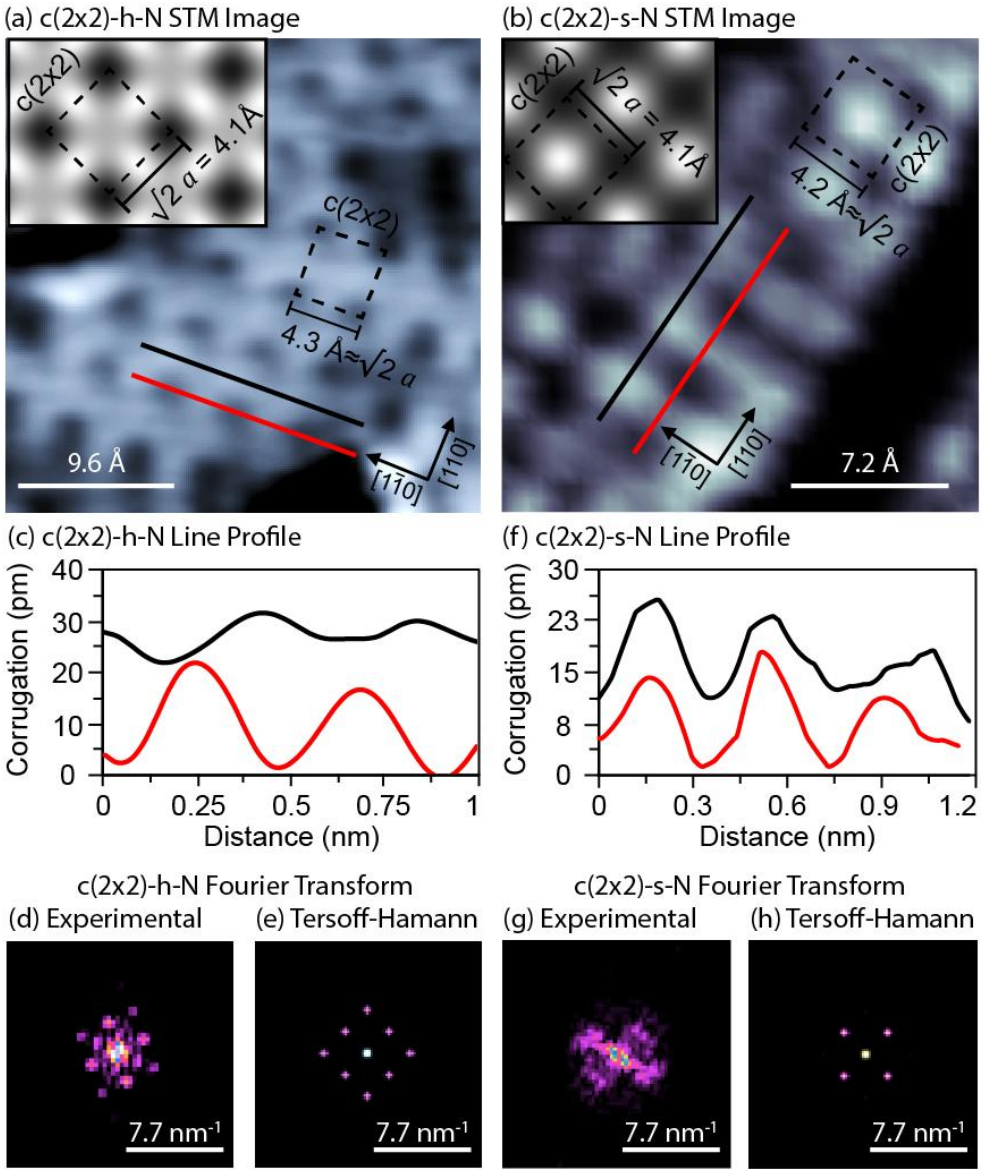

Figure 6. Experimental STM images for the (a) c(2x2)-h-N and (b) c(2x2)-s-N reconstructions. The insets show the corresponding TH-STM images (not to scale). (c) line profiles along [110] taken from (a) along the N-Cr 1st -N positions (red line) and Cr 1st -Cr 2nd-Cr 1st positions (black line) in the c(2x2)-h-N surface. (d-e) 2D-FFT of the c(2x2)-h-N structure determined from experimental and theoretical images, respectively; (f) line profiles along [$\underline{1}$10] taken from (b) along the N-Cr 2nd-N positions (red line) and Cr 1st-Cr 2nd-Cr 1st positions (black line) for the

c(2x2)-s-N surface; (g-h) 2D-FFT of the c(2x2)-s-N structure determined from experimental and theoretical images, respectively.

We point out that the c(2x2)-h-N model, where ½ ML of N atoms is located on the first monolayer, was previously used to explain the c(2x2) reconstruction [8] corresponding to Figure 6b [c(2x2)-s-N]. However, the model which makes a closer match is the one where substitutional N atoms are located at -almost- the second monolayer, about 0.2 Å above it (see Fig. 2b). This fact proves that N atoms can be found in the second monolayer as well.

Furthermore, to explain the appearance of the STM images, the local density of states of the first two Cr layers and the adsorbed nitrogen atoms were calculated for c(2x2)-h-N and c(2x2)-s-N models, and the clean Cr(001) surface. Also, the spin density of the two models was projected to the (001) plane at the same height (2.5Å) of the STM images, in order to discern the different spin contributions to the image.

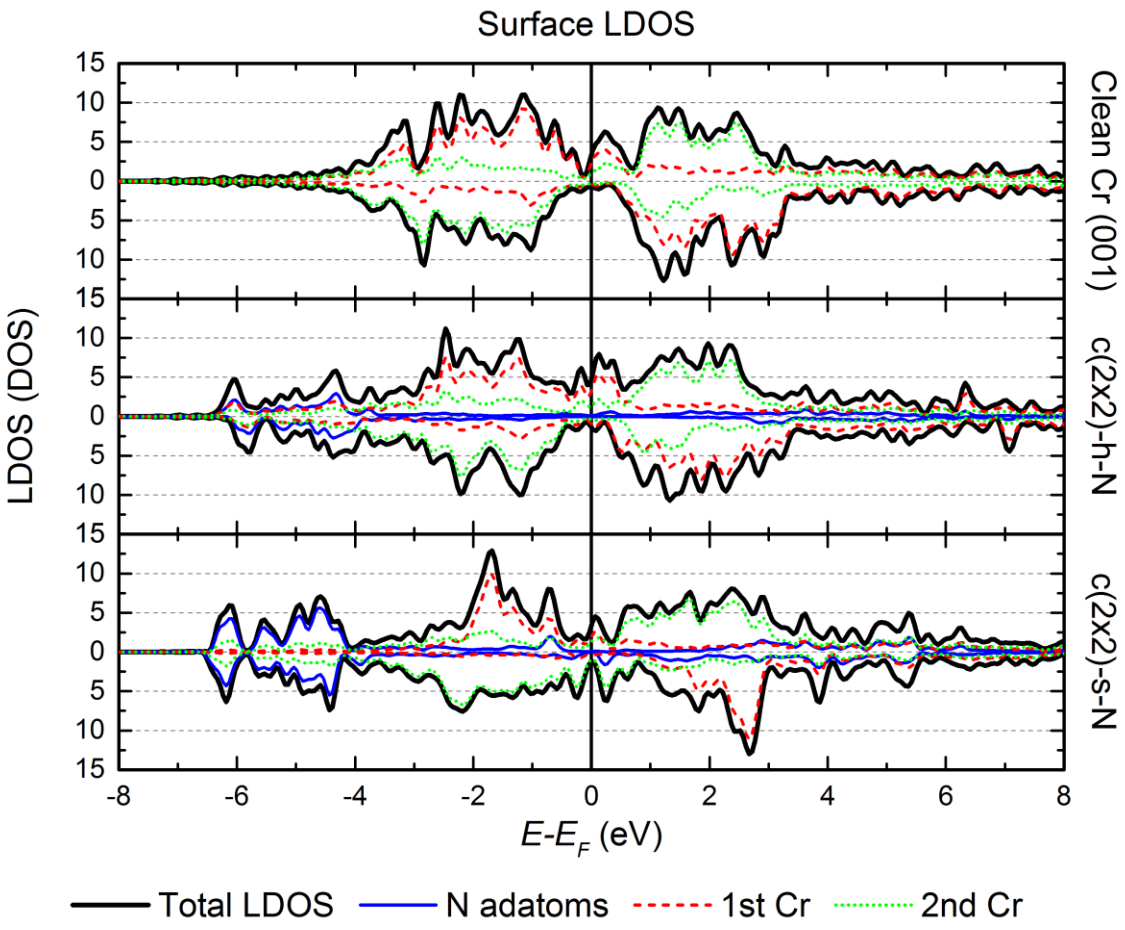

Figure 7. Local density of states of the first two layers of (top) the clean Cr (001) surface, (middle) the c(2x2)-h-N model and (bottom) the c(2x2)-s-N model. Spin-up states are shown in the top half of each plot, and spin-down in the bottom half. In all cases, the LDOS is separated in first- and second-layer Cr, and in the reconstruction models the N contribution is also separated.

In Fig 7, the LDOS is shown, where the two discontinuous lines correspond to the first two Cr layers, the thin continuous line to the N adatoms, and the bold line to the sum of these contributions. In all three cases, the metallic behavior of the surface can be clearly seen due to the states at the Fermi level. Furthermore, most occupied states of the first-layer are spin up,

while the occupied states of the second-layer are predominantly spin down, corroborating the layered aFM arrangement. Meanwhile, in the N-induced models, the N states are almost completely limited to energies between 4 and 7 eV below the Fermi Energy (E_F), while Cr has a significant density of electrons on and around E_F. This energy distribution of states confirms that indeed Cr appears as bright spots due to all of its states around E_F, while N appears as dark spots as they do not have a significant contribution of states near E_F.

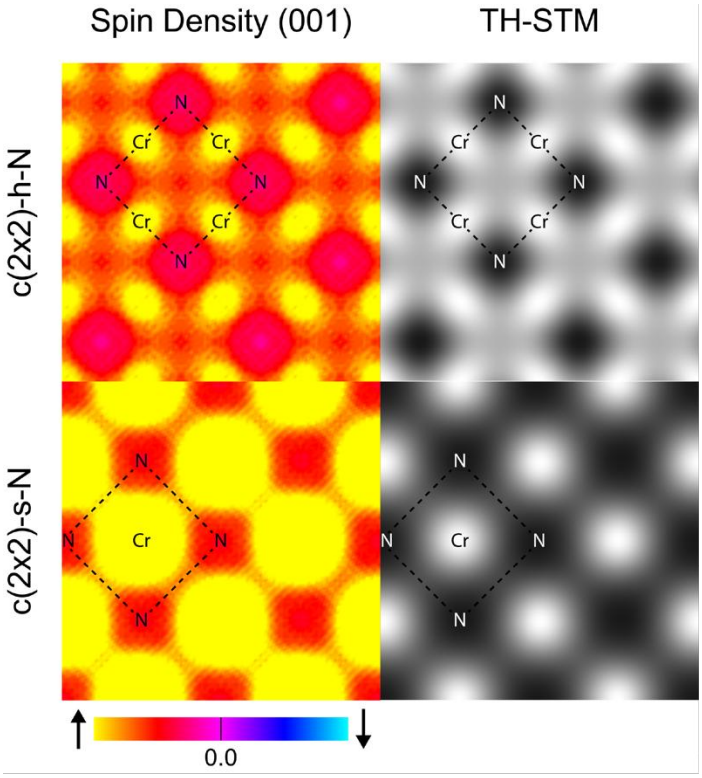

Figure 8. Spin density difference ($\rho(\uparrow) - \rho(\downarrow)$) projections on the (001) plane, at 2.5Å of the surface, for the (top) c(2x2)-h-N, and (bottom) c(2x2)-s-N models. TH-STM images for each model are shown side-by-side for comparison.

In Fig. 8, the spin density difference (SDD) projections on the (001) plane are shown for c(2x2)-h-N and c(2x2)-s-N models, side-by-side to their TH-STM images. The SDD allows us to tell

apart the contributions from the Cr 1st atoms with up-spin and the Cr 2nd with down-spin; N atoms have a slight SDD opposite from the spin of the layer they are adsorbed in (see section 3.4). For the c(2x2)-h-N model, it is clear how the Cr electron density only spreads out to unoccupied hollow sites, like the one in the middle of the superimposed reconstruction cell. Meanwhile, occupied hollow sites are dominated by N electron density, which is spin down but much less dense than the one of Cr; thus, its contribution is barely noticeable. The N density does not appear on the TH-STM because its energy is well below E_F, while the spread Cr density does appear thanks to its energy being around E_F, as discussed previously.

In the c(2x2)-s-N model, Cr density spreads out much more than in c(2x2)-h-N, as there is less Cr on the surface and N is a bit farther away. In this case, it now appears as if the N density is the one being constrained by the Cr density. Also, substitutional N becomes spin up, as it tries to compensate for the second layer spin down contribution. Nevertheless, the small spin up contribution from N does not appear in the TH-STM as its states near E_F are very few. Evidence of the spin up nature of substitutional N is presented in the next section.

3.4 Magnetic Properties

This section describes the magnetic alignments of the most stable structures with ½ ML of N atoms. As in bulk Cr, the Cr (001) surface preserves the aFM behavior along the z-axis and the magnetic moments increase towards the surface, in good agreement with a previous report [13]. When the c(2x2)-h-N reconstruction is induced, the magnetic alignment is retained. However, the absolute values of the spin densities of all Cr atoms of the first layer are increased (Figure 9a-b). A similar situation happens to the absolute values of Cr atoms of the second layer with no

nitrogen atoms on top (Figure 9a). On the other hand, the absolute values of the spin densities of Cr atoms of the second layer below N atoms show a decrease (Figure 9b).

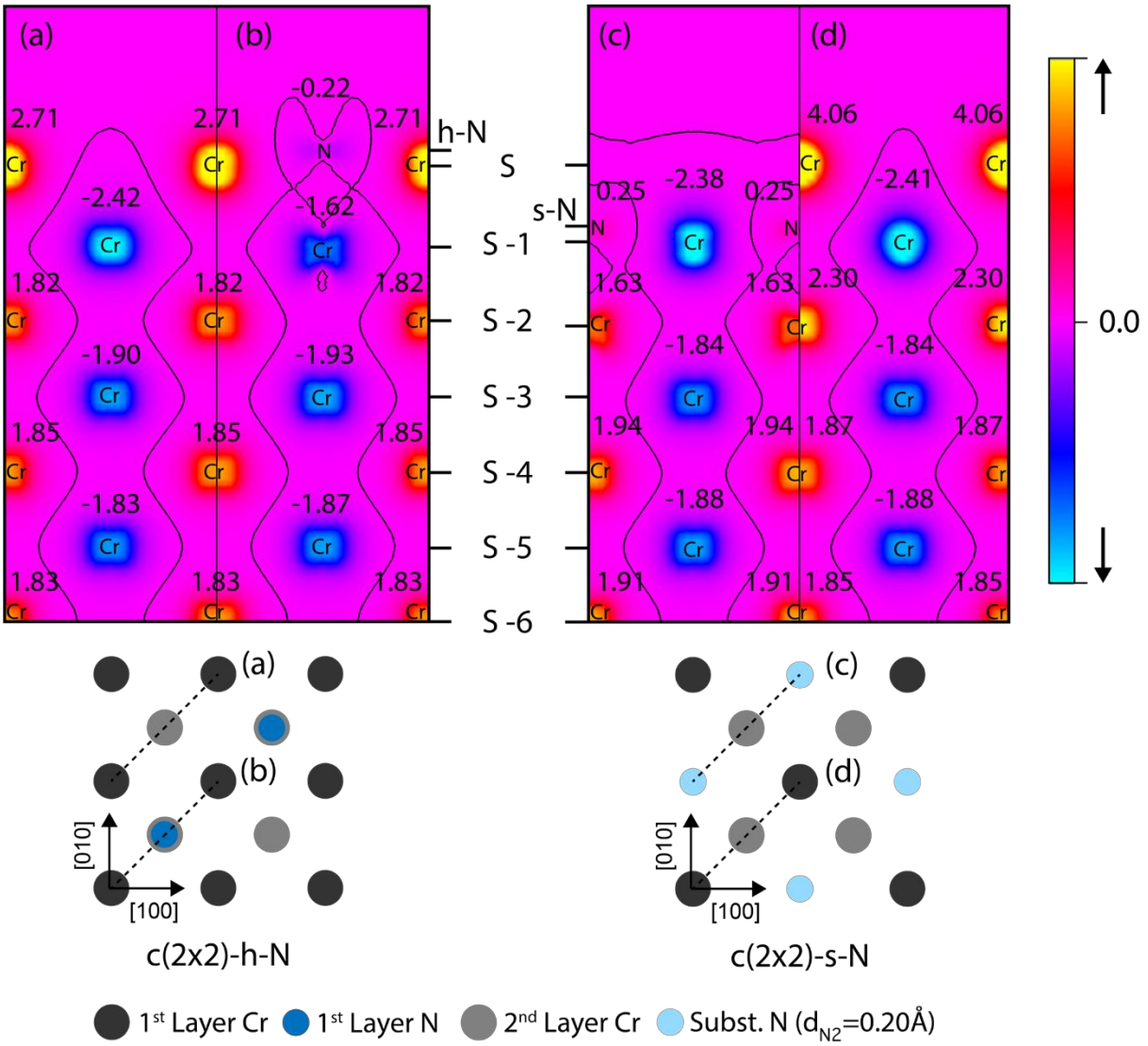

Figure 9. Calculated spin densities passing through two different (110) planes for (a) the c(2x2)-h-N and (b) the c(2x2)-s-N reconstructions. The planes shown are depicted below for each of the models. Contour lines follow $\rho(\uparrow) - \rho(\downarrow) = 0$.

As mentioned before, the magnetic alignment along the z-axis is not altered by the N incorporation; this may be due to the formation of aFM CrN units [13] as there is 1 N per

occupied (1x1) Cr cell, which exhibit this magnetic ordering below its Neél temperature of 273-278 K [27]. A similar trend is found for Cr atoms of the second and third layer of the c(2x2)-s-N reconstruction as shown in Figure 9c-d. A large increase in the spin density of the first layer can also be observed (Figure 9d). The difference in magnetic moment values between the first layer CrN units of the c(2x2)-h-N model and the second layer CrN units of c(2x2)-s-N model may be due to the largely increased magnetic moments of Cr atoms in the first layer of the c(2x2)-s-N reconstruction.

4. Conclusions

In this paper, we have studied the N adsorption/incorporation on the Cr (001) surface using spin-polarized density functional theory calculations. A surface formation energy formalism has been applied to describe the most stable adsorption sites and surface reconstructions formed by dosing the surface with N. Our main contribution is to describe the atomic arrangements of two c(2x2) reconstructions, which are stable for different growth conditions. By calculating the STM images using the Tersoff–Hamann approximation, we have shown that the c(2x2) model with N adsorbed in hollow sites [the c(2x2)-h-N] does not match the images of older STM experiments. Instead, it shows a good agreement with a new reconstruction found by J.P. Corbett and A.R. Smith. On the other hand, a new proposed model with N substituting half the surface Cr sites and relaxing into the 2nd layer matches well the experimental images of the older c(2x2) reconstruction.

Acknowledgments

We thank DGAPA-UNAM project IN101019, and Conacyt grant A1-S-9070 of the Call of Proposals for Basic Scientific Research 2017-2018 for partial financial support. We also thank support by the United States Department of Energy, Office of Basic Energy Sciences, Division of Materials Sciences and Engineering, under Award #DE-FG02-06ER46317. Calculations were performed in the DGCTIC-UNAM Supercomputing Center, project LANCAD-UNAM-DGTIC-051. E.V. thanks CONACyT for the graduate studies scholarship currently provided. N.T. thanks DGAPA-UNAM for a scholarship at the University of California, Riverside. We thank A. Rodriguez Guerrero for the technical support.

References

[1] M.N. Mukherjee, K. Sengupta, B.K. Sen, On nitride formation on chromium (001) surface, Journal of Materials Science Letters, 4 (1985) 653.

[2] M. Schmid, M. Pinczolits, W. Hebenstreit, P. Varga, The nitrogen-induced herringbone reconstruction of Cr(110), Surface Science 389 (1997) L1140.

[3] L.E. Klebanoff, R.H. Victora, L.M. Falicov, D.A. Shirley, Experimental and theoretical investigations of Cr(001) surface electronic structure, Phys. Rev. B., 32 (1985) 1997. doi:10.1103/PhysRevB.32.1997.

[4] L. Peters, A.N. Rudenko, M.I. Katsnelson, An ab-initio study of the electron-phonon coupling within a Cr(001)-surface, http://arxiv.org/abs/1801.03301v.

[5] S. Blugel, D. Pescia, P.H. Dederichs, Ferromagnetism versus antiferromagnetism of the Cr(001) surface, Physical Review B, 39 (1989) 1392.

[6] A. Kellou, H. Aourag, Diffusion, surface alloy formation, and spin alignment in Fe/Cr(001) systems and superlattices, phys. stat. sol. (b), 236 (2003) 166.

[7] M. Schmid, M. Pinczolits, W. Hebenstreit, P. Varga, Segregation of impurities on Cr (100) studied by AES and STM, Surface Science, 377-379 (1997) 1023.

[8] M. Sporn, E. Platzgummer, M. Pinczolits, W. Hebenstreit, M. Schmid, W. Hofer, P. Varga, Anti-corrugation and nitrogen c(2 x 2) on Cr(100)" STM on atomic scale and quantitative LEED, Surface Science, 396 (1998) 78.

[9] J.P. Corbett, A.R. Smith, Journal of Magnetism and Magnetic Materials, 465 (2018) 626-633. doi: 10.1016/j.jmmm.2018.06.037.

[10] D. Gall, C.-S. Shin, T. Spila, M. Odén, M.J.H. Senna, J.E. Greene, I. Petrov, Growth of single-crystal CrN on MgO(001): Effects of low-energy ion-irradiation on surface morphological evolution and physical properties, J. Appl. Phys. 91 (2002) 3589–3597. doi:10.1063/1.1446239.

[11] P.A. Anderson, R.J. Kinsey, S.M. Durbin, A. Markwitz, V.J. Kennedy, A. Asadov, W. Gao, R.J. Reeves, Magnetic and optical properties of the InCrN system, J. Appl. Phys. 98 (2005) 043903. doi:10.1063/1.1993753.

[12] A. Ney, R. Rajaram, S.S.P. Parkin, T. Kammermeier, S. Dhar, Magnetic properties of epitaxial CrN films, Appl. Phys. Lett. 89 (2006) 112504. doi:10.1063/1.2352795.

[13] K. Alam, S.M. Disseler, W.D. Ratcliff, J.A. Borchers, R. Ponce-Pérez, G.H. Cocoletzi, N. Takeuchi, A. Foley, A. Richard, D.C. Ingram, A.R. Smith, Structural and magnetic phase transitions in chromium nitride thin films grown by rf nitrogen plasma molecular beam epitaxy, Phys. Rev. B. 96 (2017) 104433. doi:10.1103/PhysRevB.96.104433.

[14] P. Eklund, S. Kerdsongpanya, B. Alling, Transition-metal-nitride-based thin films as novel energy harvesting materials, J. Mater. Chem. C. 4 (2016) 3905–3914. doi:10.1039/C5TC03891J.

[15] Z. Zhang, R. Daniel, C. Mitterer, Atomic and electronic structures of a transition layer at the CrN/Cr interface, J. Appl. Phys. 110 (2011) 043524. doi:10.1063/1.3624772.

[16] P. Giannozzi, O. Andreussi, T. Brumme, O. Bunau, M. Buongiorno Nardelli, M. Calandra, R. Car, C. Cavazzoni, D. Ceresoli, M. Cococcioni, N. Colonna, I. Carnimeo, A. Dal Corso, S. de Gironcoli, P. Delugas, R.A. DiStasio, A. Ferretti, A. Floris, G. Fratesi, G. Fugallo, R. Gebauer, U. Gerstmann, F. Giustino, T. Gorni, J. Jia, M. Kawamura, H.-Y. Ko, A. Kokalj, E. Küçükbenli, M. Lazzeri, M. Marsili, N. Marzari, F. Mauri, N.L. Nguyen, H.-V. Nguyen, A. Otero-de-la-Roza, L. Paulatto, S. Poncé, D. Rocca, R. Sabatini, B. Santra, M. Schlipf, A.P. Seitsonen, A. Smogunov, I. Timrov, T. Thonhauser, P. Umari, N. Vast, X. Wu, S. Baroni, Advanced

capabilities for materials modelling with Quantum ESPRESSO, J. Phys. Condens. Matter. 29 (2017) 465901. doi:10.1088/1361-648X/aa8f79.

[17] J.P. Perdew, K. Burke, M. Ernzerhof, Generalized Gradient Approximation Made Simple, Phys. Rev. Lett. 77 (1996) 3865–3868. doi:10.1103/PhysRevLett.77.3865.

[18] D. Vanderbilt, Soft self-consistent pseudopotentials in a generalized eigenvalue formalism, Phys. Rev. B. 41 (1990) 7892–7895. doi:10.1103/PhysRevB.41.7892.

[19] J. Tersoff, D.R. Hamann, Theory of the scanning tunneling microscope, Phys. Rev. B. 31 (1985) 805–813. doi:10.1103/PhysRevB.31.805.

[20] Villars Pierre, K. and Cenzual, eds., Cr Crystal Structure: Datasheet from "PAULING FILE Multinaries Edition–2012," Springer Materials. (2012), https://materials.springer.com/isp/crystallographic/docs/sd_0250070.

[21] P. Haas, F. Tran, P. Blaha, Calculation of the lattice constant of solids with semilocal functionals, Phys. Rev. B. 79 (2009) 085104. doi:10.1103/PhysRevB.79.085104.

[22] T. Asada, S. Blügel, G. Bihlmayer, Electronic and magnetic structure of the (001) surfaces of V, Cr, and V/Cr, Phys. Rev. B - Condens. Matter Mater. Phys. 62 (2000) R11937–R11940. doi:10.1103/PhysRevB.62.R11937.

[23] N. Takeuchi, S. Ulloa, First principles calculations of the structural and electronic properties of the ScN(0 0 1) surface, Phys. Rev. B, 65 (2002) 235307. doi: 10.1103/PhysRevB.65.235307.

[24] N. Takeuchi, Surface properties of YN(0 0 1): a first-principles calculation, Phys. Rev. B, 66 (2002) 153405. doi:10.1103/PhysRevB.66.153405.

[25] J. Guerrero-Sánchez, Andrada-Oana Mandru, Noboru Takeuchi, Gregorio H. Cocoletzi, Arthur R. Smith, Understanding the stability of Fe incorporation within Mn3N2(0 0 1) surfaces: An ab-initio study, Appl. Surf. Sci., 363 (2016) 651. doi:10.1016/j.apsusc.2015.11.263.

[26] J. Guerrero-Sánchez, Noboru Takeuchi, Antiferromagnetic MnN layer on the MnGa(001) surface, Appl. Surf. Sci., 390 (2016) 328. doi:10.1016/j.apsusc.2016.08.076.

[27] L.M. Corliss, N. Elliott, J.M. Hastings, Antiferromagnetic Structure of CrN, Physical Review. 117 (1960) 929–935. doi:10.1103/physrev.117.929.